

Oscillating 4-Polytopal Universe in Regge Calculus

REN TSUDA¹ AND TAKANORI FUJIWARA²

¹*Student Support Center, Chiba Institute of Technology, Narashino 275-0023, Japan*

²*Department of Physics, Ibaraki University, Mito 310-8512, Japan*

arXiv:2011.04120v2 [gr-qc] 17 Oct 2021

Abstract

The discretized closed Friedmann–Lemaître–Robertson–Walker (FLRW) universe with positive cosmological constant is investigated by Regge calculus. According to the Collins–Williams formalism, a hyperspherical Cauchy surface is replaced with regular 4-polytopes. Numerical solutions to the Regge equations approximate well to the continuum solution during the era of small edge length. Unlike the expanding polyhedral universe in three dimensions, the 4-polytopal universes repeat expansions and contractions. To go beyond the approximation using regular 4-polytopes we introduce pseudo-regular 4-polytopes by averaging the dihedral angles of the tessellated regular 600-cell. The degree of precision of the tessellation is called the frequency. Regge equations for the pseudo-regular 4-polytope have simple and unique expressions for any frequency. In the infinite frequency limit, the pseudo-regular 4-polytope model approaches the continuum FLRW universe.

1 Introduction

Regge calculus was proposed in 1961 to formulate Einstein's general relativity on piecewise linear manifolds [1, 2]. It is a coordinate-free discrete formulation of gravity, providing a framework in both classical and quantum studies of gravity [3]. Since Regge calculus is a highly abstract and abstruse theoretical formalism based on simplicial decomposition of space-time, further theoretical studies from various viewpoints are to be welcomed. In particular, exact results such as the Friedmann–Lemaître–Robertson–Walker (FLRW) universe and Schwarzschild space-time in the continuum theory are considered to play the role of a touchstone in Regge calculus. Thorough investigations on these systems are indispensable in making Regge calculus practical for use.

Regge calculus has been applied to the four-dimensional closed FLRW universe by Collins and Williams [4]. They considered regular polytopes (4-polytopes or polychora) as the Cauchy surfaces of the discrete FLRW universe and used, instead of simplices, truncated world-tubes evolving from one Cauchy surface to the next as the building blocks of piecewise linear space-time. Their method, called the Collins–Williams (CW) formalism, is based on the $3 + 1$ decomposition of space-time similar to the well-known Arnowitt–Deser–Misner (ADM) formalism [5–7]. Recently, Liu and Williams have extensively studied the discrete FLRW universe [8–10]. They found that a universe with regular 4-polytopes such as the Cauchy surfaces can reproduce the continuum FLRW universe to a certain degree of precision. Their solutions agree well with the continuum when the size of the universe is small, whereas the deviations from the exact results become large for a large universe.

In a previous paper [11], we investigated the three-dimensional closed FLRW universe with positive cosmological constant by the CW formalism. The main interest there was to elucidate how Regge calculus reproduces the FLRW universe in the continuum limit. In three dimensions, a spherical Cauchy surface is replaced with polyhedra. We described the five types of regular polyhedra on an equal footing by using Schläfli symbols [12]. The polyhedral universe behaves as the analytic solution of the continuum theory when the size of the universe is small, while it expands to infinity in a finite time. We further proposed a geodesic dome model to go beyond the regular polyhedra. The Regge calculus for the geodesic domes, however, becomes more and more complicated as we better and better approximate the sphere. To avoid the cumbersome tasks in carrying out Regge calculus for the geodesic dome models we introduced pseudo-regular polyhedra characterized by fractional Schläfli symbols. Regge equations for the pseudo-regular polyhedron model turned out to approximate the corresponding geodesic dome universe well. It is worth investigating whether a similar approach can be extended to higher dimensions.

In this paper we investigate the FLRW universe of four-dimensional Einstein gravity with a positive cosmological constant within the framework of the CW formalism. We consider all six types of regular 4-polytopes as the Cauchy surface in a unified way in terms of the Schläfli

	$k = 1$	$k = 0$	$k = -1$
$\Lambda > 0$	$a = \sqrt{\frac{3}{\Lambda}} \cosh\left(\sqrt{\frac{\Lambda}{3}}t\right)$	$a = \sqrt{\frac{3}{\Lambda}} \exp\left(\sqrt{\frac{\Lambda}{3}}t\right)$	$a = \sqrt{\frac{3}{\Lambda}} \sinh\left(\sqrt{\frac{\Lambda}{3}}t\right)$
$\Lambda = 0$	no solution	$a = \text{const.}$	$a = t$
$\Lambda < 0$	no solution	no solution	$a = \sqrt{-\frac{3}{\Lambda}} \sin\left(\sqrt{-\frac{\Lambda}{3}}t\right)$

Table 1: Solutions of the Friedmann equations.

symbol and compare the behaviors of the solutions with the analytic result of the continuum theory. We further propose a generalization of the Regge equations by introducing pseudo-regular polytopes, which makes the numerical analysis much easier than the conventional Regge calculus.

This paper is organized as follows: in the next section we set up the regular 4-polytopal universe in the CW formalism and introduce Regge action. Derivation of the Regge equations is given in Sect. 3. In the continuum time limit the Regge equations are reduced to differential equations. Applying the Wick rotation, we arrive at the Regge calculus analog of the Friedmann equations, describing the evolution of the 4-polytopal universe. This is done in Sect. 4. In Sect. 5 we solve the differential Regge equations numerically and compare the scale factors of the 4-polytopal universes with the continuum solution. In Sect. 6 we consider subdivision of cells of the regular 4-polytopes and propose a pseudo-regular 4-polytopal universe with a non-integer Schläfli symbol that approaches a smooth three-dimensional sphere in the continuum limit. Sect. 7 is devoted to summary and discussions. In Appendix A, the radius of the circumsphere of a regular polytope in any dimensions is considered.

2 Regge action for a regular 4-polytopal universe

We begin with a brief description of the continuum FLRW universe. The continuum action is given by

$$S = \frac{1}{16\pi} \int d^4x \sqrt{-g} (R - 2\Lambda). \quad (2.1)$$

In four dimensions, the Einstein equations have an evolving universe as a solution for the ansatz

$$ds^2 = -dt^2 + a(t)^2 \left[\frac{dr^2}{1 - kr^2} + r^2 (d\theta^2 + \sin^2 \theta d\varphi^2) \right], \quad (2.2)$$

where $a(t)$ is the so-called scale factor in cosmology. It is subject to the Friedmann equations

$$\dot{a}^2 = \frac{\Lambda}{3} a^2 - k, \quad \ddot{a} = \frac{\Lambda}{3} a. \quad (2.3)$$

The curvature parameter $k = 1, 0, -1$ corresponds to space being spherical, Euclidean, or hyperbolic, respectively. The relations between the solutions and curvature parameter are summarized in Table 1 with the proviso that the behaviors of the universes are restricted to expanding at the beginning for the initial condition $a(0) = \min a(t)$. Of these, our concern is the spherical universe with three-dimensional spheres as the Cauchy surfaces. All the time dependence of the universe is in the scale factor $a(t)$, which expresses the curvature radius of the Cauchy surface. In Regge calculus we will replace the three-dimensional sphere with a regular 4-polytope.

Before entering into details of the 4-polytopal universe, let us briefly summarize the essence of Regge calculus: in Regge calculus, an analog of the Einstein–Hilbert action is given by the Regge action [13]

$$S_{\text{Regge}} = \frac{1}{8\pi} \left(\sum_{i \in \{\text{hinges}\}} \varepsilon_i A_i - \Lambda \sum_{i \in \{\text{blocks}\}} V_i \right), \quad (2.4)$$

where A_i is the volume of a hinge, ε_i the deficit angle around the hinge A_i , and V_i the volume of a building block of the piecewise linear manifold. In four dimensions the hinges are the lattice planes, or equivalently the faces of the 4-simplices, and A_i is nothing but the face area. Regge’s original derivation is concerned with a simplicial lattice, so that it describes the gravity as simplicial geometry. In fact this formalism can easily be generalized to arbitrary lattice geometries. We can fully triangulate the non-simplicial flat blocks by adding extra hinges with vanishing deficit angles without affecting the Regge action.

The fundamental variables in Regge calculus are the edge lengths l_i . Varying the Regge action with respect to l_i , we obtain the Regge equations

$$\sum_{i \in \{\text{hinges}\}} \varepsilon_i \frac{\partial A_i}{\partial l_j} - \Lambda \sum_{i \in \{\text{blocks}\}} \frac{\partial V_i}{\partial l_j} = 0. \quad (2.5)$$

Note that there is no need to carry out the variation of the deficit angles owing to the Schläfli identity [14, 15]

$$\sum_{i \in \{\text{hinges}\}} A_i \frac{\partial \varepsilon_i}{\partial l_j} = 0. \quad (2.6)$$

We now turn to 4-polytopal universes. Following the CW formalism, we replace the hyperspherical Cauchy surface by a regular 4-polytope. It would be helpful to begin with a description of regular 4-polytopes [12]. As regular polyhedra in three dimensions, a regular 4-polytope can be obtained by gluing three-dimensional cells of congruent regular polyhedra. Any regular 4-polytope can be specified by the Schläfli symbol $\{p, q, r\}$, where $\{p, q\}$ stands for the Schläfli symbol of a cell and r the number of cells having an edge of a cell in common. It is known that there are only six types of regular 4-polytopes: 5-cell, 8-cell, 16-cell, 24-cell,

	5-cell	8-cell	16-cell	24-cell	120-cell	600-cell
N_3	5	8	16	24	120	600
N_2	10	24	32	96	720	1200
N_1	10	32	24	96	1200	720
N_0	5	16	8	24	600	120
$\{p, q, r\}$	$\{3, 3, 3\}$	$\{4, 3, 3\}$	$\{3, 3, 4\}$	$\{3, 4, 3\}$	$\{5, 3, 3\}$	$\{3, 3, 5\}$

Table 2: The six regular polytopes in four dimensions.

120-cell, and 600-cell, as listed in Table 2. Incidentally, this can be extended inductively to polytopes in arbitrary dimensions. In general, a D -polytope can be denoted by a set of $D - 1$ parameters $\{p_2, \dots, p_D\}$.

Let us denote the numbers of vertices, edges, faces, and cells of a regular 4-polytope $\{p, q, r\}$ by N_0 , N_1 , N_2 , and N_3 , respectively. They satisfy $n_2(q, r) N_0 = n_0(p, q) N_3$, $r N_1 = n_1(p, q) N_3$, and $2N_2 = n_2(p, q) N_3$, where $n_0(p, q)$, $n_1(p, q)$, and $n_2(p, q)$ are the numbers of vertices, edges, and faces of a regular polyhedron $\{p, q\}$, respectively. These completely determine the ratios $N_{0,1,2}/N_3$ as

$$\frac{N_0}{N_3} = \frac{n_0(p, q)}{n_2(q, r)} = \frac{p(2q + 2r - qr)}{r(2p + 2q - pq)}, \quad (2.7)$$

$$\frac{N_1}{N_3} = \frac{n_1(p, q)}{r} = \frac{2pq}{r(2p + 2q - pq)}, \quad (2.8)$$

$$\frac{N_2}{N_3} = \frac{n_2(p, q)}{2} = \frac{2q}{2p + 2q - pq}, \quad (2.9)$$

and have a consistency with Schläfli's formula

$$N_0 - N_1 + N_2 - N_3 = 0. \quad (2.10)$$

Furthermore, it is known that N_3 is given by Coxeter's formula [12, 16]

$$N_3 = \frac{32h_{pqr}}{pn_2(p, q) \left[12 - p - 2q - r + 4 \left(\frac{1}{p} + \frac{1}{r} \right) \right]}, \quad (2.11)$$

where h_{pqr} is a positive integer known as the Petrie number. It is related to the largest root of the quartic equation

$$x^4 - \left(\cos^2 \frac{\pi}{p} + \cos^2 \frac{\pi}{q} + \cos^2 \frac{\pi}{r} \right) x^2 + \cos^2 \frac{\pi}{p} \cos^2 \frac{\pi}{r} = 0 \quad (2.12)$$

by $x = \cos \frac{\pi}{h_{pqr}}$. Equations (2.7)–(2.9) and (2.11) determine $N_{0,1,2,3}$. As we shall see, the ratios in Eqs (2.7)–(2.9) are sufficient in writing the Regge equations. In Table 2 we summarize the properties of regular 4-polytopes for the reader's reference.

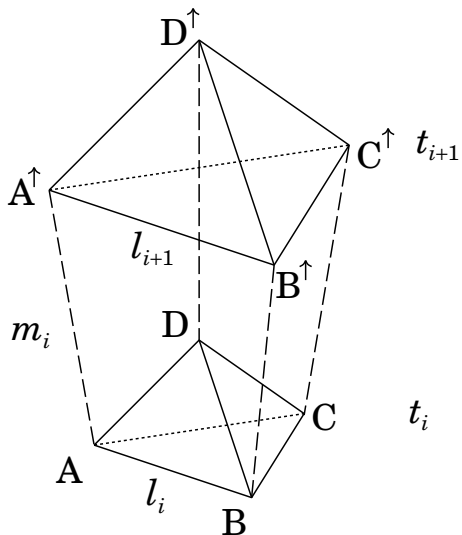


Figure 1: The i th frustum as the fundamental building block of a 4-polytopal universe for $p = q = 3$. A cell of regular tetrahedron $ABCD$ with edge length l_i at time t_i evolves into a cell $A^\uparrow B^\uparrow C^\uparrow D^\uparrow$ with edge length l_{i+1} at t_{i+1} .

As depicted in Fig. 1, the fundamental building blocks of space-time in the Regge calculus are world-tubes of four-dimensional frustums with the regular polyhedra $\{p, q\}$ as the upper and lower cells, and with $n_2(p, q)$ lateral cells which are three-dimensional frustums with p -sided regular polygons as the upper and lower faces. In Fig. 1 the lateral cells are the three-dimensional frustums $ABC-A^\uparrow B^\uparrow C^\uparrow$, $ABD-A^\uparrow B^\uparrow D^\uparrow$, $ACD-A^\uparrow C^\uparrow D^\uparrow$, and $BCD-B^\uparrow C^\uparrow D^\uparrow$.

Following the regular polyhedron models [11], we assume that the lower and upper cells of a block separately lie in a time-slice and every strut between them has equal length. The whole space-time is then obtained by gluing such frustums cell-by-cell without a break. There are two types of fundamental variables: the lengths of the edges, l_i , and those of the struts, m_i . Since the hinges are two-dimensional faces in four dimensions, there are only two types of hinges. One is a face of a regular polyhedron in a time-slice, like $\triangle ABC$ in Fig. 1. We call it simply a “polygon” and denote by $A_i^{(p)}$ the area of the polygon on the i th Cauchy surface at time t_i . The other type of hinge is an isosceles trapezoidal face of lateral cells between the consecutive Cauchy surfaces, such as $\square ABB^\uparrow A^\uparrow$ in Fig. 1. We call them “trapezoid” and denote by $A_i^{(t)}$ the area of the trapezoid between the Cauchy surfaces at t_i and t_{i+1} .

With these in mind, the Regge action (2.4) can be written as

$$S_{\text{Regge}} = \frac{1}{8\pi} \sum_i \left(N_1 A_i^{(t)} \varepsilon_i^{(t)} + N_2 A_i^{(p)} \varepsilon_i^{(p)} - N_3 \Lambda V_i \right), \quad (2.13)$$

where $\varepsilon_i^{(t)}$ and $\varepsilon_i^{(p)}$ stand for the deficit angles around the trapezoid and polygon, respectively, and V_i is the world-volume of the i th frustum. The sum on the right-hand side is taken over

the time-slices. As we show in the next section, the deficit angles, areas, and volume are given in terms of the lengths of the edges and struts.

3 Regge equations

The Regge equations can be obtained by varying the action (2.13) with respect to the fundamental variables m_i and l_i . Note that two adjacent trapezoids $A_i^{(t)}$ and $A_{i-1}^{(t)}$ have the edge l_i in common, as do V_i and V_{i-1} . Then, Eq. (2.5) can be written as

$$\frac{\partial A_i^{(t)}}{\partial m_i} \varepsilon_i^{(t)} = \frac{r(2p+2q-pq)}{2pq} \Lambda \frac{\partial V_i}{\partial m_i}, \quad (3.1)$$

$$\frac{\partial A_i^{(t)}}{\partial l_i} \varepsilon_i^{(t)} + \frac{\partial A_{i-1}^{(t)}}{\partial l_i} \varepsilon_{i-1}^{(t)} = -\frac{r}{p} \frac{\partial A_i^{(p)}}{\partial l_i} \varepsilon_i^{(p)} + \frac{r(2p+2q-pq)}{2pq} \Lambda \left(\frac{\partial V_i}{\partial l_i} + \frac{\partial V_{i-1}}{\partial l_i} \right). \quad (3.2)$$

In the context of the ADM formalism, Eq. (3.1) corresponds to the Hamiltonian constraint and Eq. (3.2) to the evolution equation.

The deficit angles, areas of the hinges, and volume of the frustum can be expressed in terms of l and m . For the sake of lucidness in defining lengths and angles, we temporarily assume the metric in each building block to be flat Euclidean so that the geometric objects such as lengths and angles are obvious. The equations of motion in Lorentzian geometry can be achieved by Wick rotation.

We first focus our attention on a trapezoidal hinge $h_i^{(t)} = \text{BB}^\dagger \text{D}^\dagger \text{D}$ of the i th frustum, the shaded area of Fig. 2(a). One sees that the two lateral cells $c_{Ai}^{(l)} = \text{ABD}-\text{A}^\dagger \text{B}^\dagger \text{D}^\dagger$ and $c_{Ci}^{(l)} = \text{BCD}-\text{B}^\dagger \text{C}^\dagger \text{D}^\dagger$ have the hinge $h_i^{(t)}$ in common as a face. We can find a unit normal vector \mathbf{u}_A to the cell $c_{Ai}^{(l)}$. It is orthogonal to vectors $\overrightarrow{\text{BA}}, \overrightarrow{\text{BD}},$ and $\overrightarrow{\text{BB}^\dagger}$. Similarly, we denote by \mathbf{u}_C a unit normal to the cell $c_{Ci}^{(l)}$. Then the dihedral angle θ_i between the two lateral cells is defined by

$$\theta_i = \arccos \mathbf{u}_A \cdot \mathbf{u}_C. \quad (3.3)$$

(See Fig. 2b.) This is explicitly written as

$$\theta_i = \arccos \frac{4 \left(\sin^2 \frac{\pi}{p} - 2 \cos^2 \frac{\pi}{q} \right) m_i^2 + \delta l_i^2 \cos \frac{2\pi}{q}}{4m_i^2 \sin^2 \frac{\pi}{p} - \delta l_i^2}, \quad (3.4)$$

where $\delta l_i = l_{i+1} - l_i$. The deficit angle $\varepsilon_i^{(t)}$ around the hinge $h_i^{(t)}$ can be found by noting the fact that there are r frustums that have the trapezoid in common as illustrated in Fig. 2(c). We thus obtain

$$\varepsilon_i^{(t)} = 2\pi - r\theta_i. \quad (3.5)$$

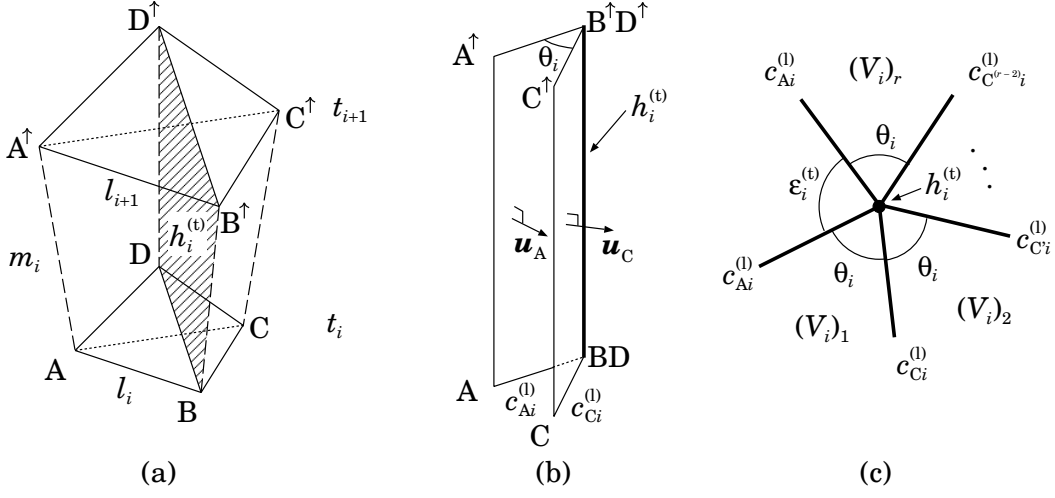


Figure 2: (a) two lateral cells $c_{Ai}^{(l)}$ and $c_{Ci}^{(l)}$ meeting at the trapezoidal hinge $h_i^{(t)}$, (b) dihedral angle between $c_{Ai}^{(l)}$ and $c_{Ci}^{(l)}$, and (c) deficit angle around the hinge $h_i^{(t)}$ made by r frustums $(V_i)_1, \dots, (V_i)_r$ having $h_i^{(t)}$ as a lateral face in common. Though Figure (a) assumes an evolution of a regular tetrahedron, any polyhedron can be used.

We next pick up a pair of polygonal hinges $h_i^{(p)} = ABD$ and $h_{i+1}^{(p)} = A^\uparrow B^\uparrow D^\uparrow$ in the i th frustum as depicted in Fig. 3(a). They are the upper and lower faces of the lateral cell $c_{Ai}^{(l)}$ defined above. The lateral cell $c_{Ai}^{(l)}$ and the base cell $c_{Ci}^{(b)} = ABCD$ meet at the hinge $h_i^{(p)}$. We denote the dihedral angle between them by ϕ_i^\uparrow . Similarly, we write the dihedral angle between $c_{Ai}^{(l)}$ and $c_{C_{i+1}}^{(b)} = A^\uparrow B^\uparrow C^\uparrow D^\uparrow$ by ϕ_{i+1}^\downarrow . Since $c_{Ci}^{(b)}$ and $c_{C_{i+1}}^{(b)}$ are parallel to each other, the dihedral angles satisfy

$$\phi_i^\uparrow + \phi_{i+1}^\downarrow = \pi. \quad (3.6)$$

(See Fig. 3b.) The dihedral angle ϕ_i^\downarrow can be obtained by the way just explained for θ_i as

$$\phi_i^\downarrow = \arccos \frac{\delta l_{i-1} \cos \frac{\pi}{p} \cos \frac{\pi}{q}}{\sqrt{\left(\sin^2 \frac{\pi}{p} - \cos^2 \frac{\pi}{q}\right) \left(4m_{i-1}^2 \sin^2 \frac{\pi}{p} - \delta l_{i-1}^2\right)}}. \quad (3.7)$$

To find the deficit angle around the hinge $h_i^{(p)}$, we must take account of four frustums that have $h_i^{(p)}$ in common: two adjacent V_i in the future side and two adjacent V_{i-1} in the past side, as schematically illustrated in Fig. 3(c). Then, the deficit angle $\epsilon_i^{(p)}$ can be written as

$$\epsilon_i^{(p)} = 2\pi - 2 \left(\phi_i^\uparrow + \phi_i^\downarrow \right) = 2\delta\phi_i^\downarrow, \quad (3.8)$$

where we have introduced $\delta\phi_i^\downarrow = \phi_{i+1}^\downarrow - \phi_i^\downarrow$.

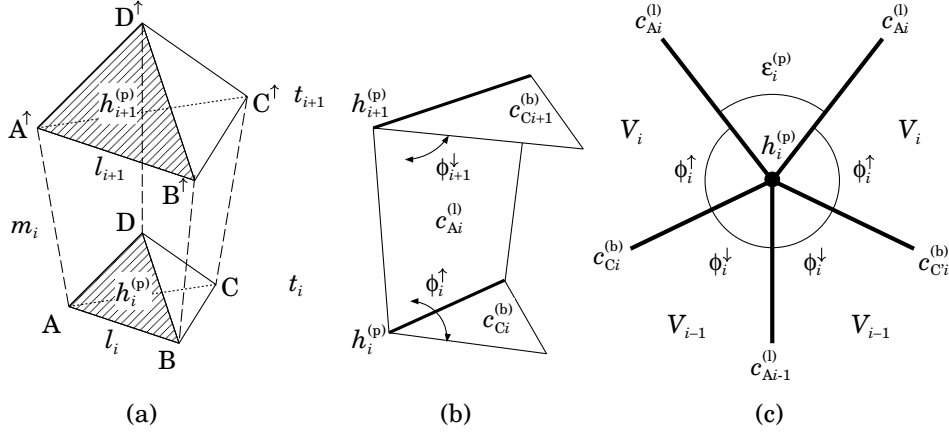


Figure 3: (a) two polygonal hinges $h_i^{(p)}$ and $h_{i+1}^{(p)}$ in the i th frustum, (b) dihedral angles ϕ_i^\uparrow and ϕ_{i+1}^\downarrow , and (c) deficit angle $\varepsilon_i^{(p)}$.

The areas of the hinges and the volume of the frustum can also be expressed in terms of l and m . The areas of a trapezoid $A_i^{(t)}$ and a polygon $A_i^{(p)}$ can be written as

$$A_i^{(t)} = \frac{1}{2} (l_{i+1} + l_i) \sqrt{m_i^2 - \frac{1}{4} \delta l_i^2}, \quad (3.9)$$

$$A_i^{(p)} = \frac{p}{4} l_i^2 \cot \frac{\pi}{p}. \quad (3.10)$$

The volume of the i th frustum is given by

$$V_i = \frac{pq \cot^2 \frac{\pi}{p} \cos \frac{\pi}{q} (l_{i+1} + l_i) (l_{i+1}^2 + l_i^2)}{24 (2p + 2q - pq) \sqrt{\sin^2 \frac{\pi}{p} - \cos^2 \frac{\pi}{q}}} \sqrt{m_i^2 - \frac{\sin^2 \frac{\pi}{q}}{4 (\sin^2 \frac{\pi}{p} - \cos^2 \frac{\pi}{q})} \delta l_i^2}. \quad (3.11)$$

Inserting these expressions into the Regge equations (3.1) and (3.2), we obtain a set of

recurrence relations:

$$\begin{aligned}
\frac{\varepsilon_i^{(t)}}{\sqrt{4m_i^2 - \delta l_i^2}} &= \frac{r\Lambda}{24} \frac{(l_{i+1}^2 + l_i^2) \cot^2 \frac{\pi}{p} \cos \frac{\pi}{q}}{\sqrt{4m_i^2 \left(\sin^2 \frac{\pi}{p} - \cos^2 \frac{\pi}{q} \right) - \sin^2 \frac{\pi}{q} \delta l_i^2}}, \tag{3.12} \\
&\sqrt{4m_i^2 - \delta l_i^2} \varepsilon_i^{(t)} + \sqrt{4m_{i-1}^2 - \delta l_{i-1}^2} \varepsilon_{i-1}^{(t)} \\
&+ \frac{l_{i+1}^2 - l_i^2}{\sqrt{4m_i^2 - \delta l_i^2}} \varepsilon_i^{(t)} - \frac{l_i^2 - l_{i-1}^2}{\sqrt{4m_{i-1}^2 - \delta l_{i-1}^2}} \varepsilon_{i-1}^{(t)} + 2r \cot \frac{\pi}{p} l_i \varepsilon_i^{(p)} \\
&= \frac{r\Lambda \cot^2 \frac{\pi}{p} \cos \frac{\pi}{q}}{24 \left(\sin^2 \frac{\pi}{p} - \cos^2 \frac{\pi}{q} \right)} \left[(l_{i+1}^2 + 2l_{i+1}l_i + 3l_i^2) \sqrt{4m_i^2 \left(\sin^2 \frac{\pi}{p} - \cos^2 \frac{\pi}{q} \right) - \sin^2 \frac{\pi}{q} \delta l_i^2} \right. \\
&+ (3l_i^2 + 2l_i l_{i-1} + l_{i-1}^2) \sqrt{4m_{i-1}^2 \left(\sin^2 \frac{\pi}{p} - \cos^2 \frac{\pi}{q} \right) - \sin^2 \frac{\pi}{q} \delta l_{i-1}^2} \\
&\left. + \frac{(l_{i+1}^4 - l_i^4) \sin^2 \frac{\pi}{q}}{\sqrt{4m_i^2 \left(\sin^2 \frac{\pi}{p} - \cos^2 \frac{\pi}{q} \right) - \sin^2 \frac{\pi}{q} \delta l_i^2}} - \frac{(l_i^4 - l_{i-1}^4) \sin^2 \frac{\pi}{q}}{\sqrt{4m_{i-1}^2 \left(\sin^2 \frac{\pi}{p} - \cos^2 \frac{\pi}{q} \right) - \sin^2 \frac{\pi}{q} \delta l_{i-1}^2}} \right]. \tag{3.13}
\end{aligned}$$

These are non-linear recurrence relations for the edge and strut lengths l_i and m_i . Evolution of the polytopal universe can be investigated by taking the continuum time limit as in Refs. [4, 8–10].

4 Continuum time limit

We are interested in the evolution of a model universe with a regular polytope as the Cauchy surfaces. In continuum theory, Cauchy surfaces are defined as slices of space-time by constant times. In the FLRW universe, the time axis is taken to be orthogonal to the Cauchy surfaces. This seems to correspond to choosing the time axis to be orthogonal to the Cauchy cells. One can identify the distance between the centers of circumspheres of the two Cauchy cells in Fig. 1 with the Euclidean time interval $\delta t_i = t_{i+1} - t_i$. This works for Cauchy cells of regular polyhedrons [8, 9]. Later in this paper we consider Cauchy surfaces that are not necessarily regular polytopes. For general polytopal substitutions for 3-spheres as Cauchy surfaces, however, distances between two temporally consecutive Cauchy cells vary cell by cell. One cannot identify the temporal distances with a common time interval δt_i , as noted in Ref. [11] for polyhedral universe.

We avoid the subtleties in identifying the time coordinate by supposing a fictitious point material in a state of rest spatially at each vertex of the polytopal Cauchy surface. Taking t_i as the proper time of a clock standing by the fictitious material particle, we can identify

strut length m_i with the time interval

$$m_i = \delta t_i. \quad (4.1)$$

The time axis is not defined to be orthogonal to the polytopal Cauchy surfaces. The orthogonality of the temporal axis with the spatial ones is restored in the continuum limit. We further choose all the time intervals δt_i to be equal and then take the continuum time limit $\delta t_i \rightarrow dt$. The edge lengths can be regarded as a smooth function of time $l_i \rightarrow l(t)$, and

$$\delta l_i = \frac{\delta l_i}{\delta t_i} \delta t_i \rightarrow \dot{l} dt, \quad (4.2)$$

where $\dot{l} = dl/dt$. It is straightforward to take the continuum time limit for Eqs. (3.12) and (3.13). We find

$$\frac{\varepsilon^{(t)}}{\sqrt{4 - \dot{l}^2}} = \frac{r\Lambda}{12} \frac{l^2 \cot^2 \frac{\pi}{p} \cos \frac{\pi}{q}}{\sqrt{4 \left(\sin^2 \frac{\pi}{p} - \cos^2 \frac{\pi}{q} \right) - \dot{l}^2 \sin^2 \frac{\pi}{q}}}, \quad (4.3)$$

$$\begin{aligned} & \sqrt{4 - \dot{l}^2} \varepsilon^{(t)} + \frac{d}{dt} \left(\frac{\dot{l} l}{\sqrt{4 - \dot{l}^2}} \varepsilon^{(t)} \right) + 2rl \cot \frac{\pi}{p} \dot{\phi}^\downarrow \\ &= \frac{r\Lambda}{12} \frac{\cot^2 \frac{\pi}{p} \cos \frac{\pi}{q}}{\sin^2 \frac{\pi}{p} - \cos^2 \frac{\pi}{q}} \left[3l^2 \sqrt{4 \left(\sin^2 \frac{\pi}{p} - \cos^2 \frac{\pi}{q} \right) - \dot{l}^2 \sin^2 \frac{\pi}{q}} \right. \\ & \quad \left. + \frac{d}{dt} \left(\frac{l^3 \dot{l} \sin^2 \frac{\pi}{q}}{\sqrt{4 \left(\sin^2 \frac{\pi}{p} - \cos^2 \frac{\pi}{q} \right) - \dot{l}^2 \sin^2 \frac{\pi}{q}}} \right) \right], \end{aligned} \quad (4.4)$$

where $\varepsilon^{(t)}$ and $\dot{\phi}^\downarrow$ are, respectively, the continuum time limits of Eqs. (3.5) and (3.7)

$$\varepsilon^{(t)} = 2\pi - r \arccos \frac{4 \left(\sin^2 \frac{\pi}{p} - 2 \cos^2 \frac{\pi}{q} \right) + \dot{l}^2 \cos \frac{2\pi}{q}}{4 \sin^2 \frac{\pi}{p} - \dot{l}^2}, \quad (4.5)$$

$$\dot{\phi}^\downarrow = \frac{d}{dt} \arccos \frac{\dot{l} \cos \frac{\pi}{p} \cos \frac{\pi}{q}}{\sqrt{\left(\sin^2 \frac{\pi}{p} - \cos^2 \frac{\pi}{q} \right) \left(4 \sin^2 \frac{\pi}{p} - \dot{l}^2 \right)}}. \quad (4.6)$$

Since we have fixed the strut lengths by Eq. (4.1), they disappear from the Regge equations. Furthermore, substituting Eqs. (4.3) and (4.6) into the evolution equation (4.4), it can be simplified as

$$\ddot{l} = -\frac{\Lambda}{3} l \left(1 - \frac{\dot{l}^2}{4 \sin^2 \frac{\pi}{p}} \right) \left[1 - \frac{1}{4} \dot{l}^2 + \frac{1}{2} \frac{\dot{l} \ddot{l} \cos^2 \frac{\pi}{p}}{4 \left(\sin^2 \frac{\pi}{p} - \cos^2 \frac{\pi}{q} \right) - \dot{l}^2 \sin^2 \frac{\pi}{q}} \right]. \quad (4.7)$$

One can easily verify that this is consistent with the Hamiltonian constraint (4.3). In other words, the Hamiltonian constraint (4.3) can be obtained as the first integral of the evolution equation (4.7) for the initial conditions

$$l(0) = l_0 = \sqrt{\frac{12}{r\Lambda} (2\pi - r\theta_0) \cot \frac{\theta_0}{2} \tan \frac{\pi}{p}}, \quad \dot{l}(0) = 0, \quad (4.8)$$

where $\theta_0 = 2 \arcsin [\cos(\pi/q) / \sin(\pi/p)]$ stands for a dihedral angle of the regular polyhedron $\{p, q\}$. The cosmological constant must be positive for regular 4-polytopes as we see from Eq. (4.8). This implies that the space-time is de Sitter-like. The 4-polytopal universe cannot expand from or contract to a point but has minimum edge length l_0 , as does the continuum solution, as we shall see below.

So far we have worked with piecewise linear space-time with Euclidean signature. To argue the evolution of space-time we move to the Minkowskian signature by Wick rotation. This can be done simply by letting $\dot{l}^2, \ddot{l} \rightarrow -\dot{l}^2, -\ddot{l}$ in Eqs. (4.3) and (4.7). We thus obtain

$$\begin{aligned} & 2\pi - r \arccos \frac{4 \left(\sin^2 \frac{\pi}{p} - 2 \cos^2 \frac{\pi}{q} \right) - \dot{l}^2 \cos \frac{2\pi}{q}}{4 \sin^2 \frac{\pi}{p} + \dot{l}^2} \\ &= \frac{r\Lambda}{12} \dot{l}^2 \sqrt{\frac{4 + \dot{l}^2}{4 \left(\sin^2 \frac{\pi}{p} - \cos^2 \frac{\pi}{q} \right) + \dot{l}^2 \sin^2 \frac{\pi}{q}}} \cot^2 \frac{\pi}{p} \cos \frac{\pi}{q}, \end{aligned} \quad (4.9)$$

$$\ddot{l} = \frac{\Lambda}{3} l \left(1 + \frac{\dot{l}^2}{4 \sin^2 \frac{\pi}{p}} \right) \left[1 + \frac{1}{4} \dot{l}^2 - \frac{1}{2} \frac{\ddot{l} \cos^2 \frac{\pi}{p}}{4 \left(\sin^2 \frac{\pi}{p} - \cos^2 \frac{\pi}{q} \right) + \dot{l}^2 \sin^2 \frac{\pi}{q}} \right]. \quad (4.10)$$

From the evolution equation (4.10) we see that the acceleration \ddot{l} is always positive. Hence the polytopal universe, as the continuum solution, exhibits accelerated expansion or decelerated contraction with the minimum edge length (4.8). The universe, however, reaches a maximum size in a finite period of time as we shall see in the next section.

As a consistency check, let us consider the case of a vanishing cosmological constant before turning to a detailed exposition of the behavior of the polytopal universe described by the evolution equation (4.10). In the absence of a cosmological constant, the Hamiltonian constraint (4.9) becomes

$$\dot{l}^2 = \frac{8 \left(\sin^2 \frac{\pi}{p} \sin^2 \frac{\pi}{r} - \cos^2 \frac{\pi}{q} \right)}{\cos \frac{2\pi}{q} + \cos \frac{2\pi}{r}} = \text{const.} \geq 0. \quad (4.11)$$

There is no convex regular 4-polytope that has a Schläfli symbol satisfying this inequality. In the case of $\dot{l}^2 = 0$, it admits $\{p, q, r\} = \{4, 3, 4\}$ which gives a flat Cauchy surface corresponding to the Minkowski metric. Moreover, in the case of $\dot{l}^2 > 0$, a Schläfli symbol satisfying this inequality stands for a regular lattice of open Cauchy surface of constant negative curvature. These results are consistent with solutions of the Friedmann equations (see Table 1).

5 Numerical solution

In this section, we solve the Hamiltonian constraint (4.9) numerically and examine the behaviors of the regular 4-polytopal universes. It is convenient to use the continuum time limit of the dihedral angle (3.4). Let us denote it by θ :

$$\theta = \arccos \frac{4 \left(\sin^2 \frac{\pi}{p} - 2 \cos^2 \frac{\pi}{q} \right) - \dot{l}^2 \cos \frac{2\pi}{q}}{4 \sin^2 \frac{\pi}{p} + \dot{l}^2}. \quad (5.1)$$

Then l and \dot{l} can be expressed as

$$\dot{l}^2 = \frac{4 \left(\cos^2 \frac{\pi}{q} - \sin^2 \frac{\pi}{p} \sin^2 \frac{\theta}{2} \right)}{\sin^2 \frac{\theta}{2} - \cos^2 \frac{\pi}{q}}, \quad (5.2)$$

$$l^2 = \frac{12}{r\Lambda} (2\pi - r\theta) \tan^2 \frac{\pi}{p} \cot \frac{\theta}{2}. \quad (5.3)$$

The first of these can be obtained directly from Eq. (5.1). The second can be derived from the Hamiltonian constraint (4.9) by replacing \dot{l}^2 with Eq. (5.1). Since $\dot{l}^2 \geq 0$, the dihedral angle varies in the range $\theta_q \leq \theta \leq \theta_0$, where $\theta_q = (q-2)\pi/q$. The velocity \dot{l} diverges for $\theta = \theta_q$, while the edge length l approaches a finite value $l = l_{p,q,r}$, where

$$l_{p,q,r} = \sqrt{\frac{12\pi}{\Lambda} \left(\frac{2}{q} + \frac{2}{r} - 1 \right) \tan \frac{\pi}{q} \tan \frac{\pi}{p}}. \quad (5.4)$$

This is contrasted with the polyhedral universe [11], where both l and \dot{l} diverge at a finite time.

To see these in more detail we eliminate the edge length from Eqs. (5.2) and (5.3) to obtain

$$\dot{\theta} = \mp \frac{2 \sin \frac{\theta}{2} \csc \frac{\theta_0}{2}}{2\pi - r(\theta - \sin \theta)} \sqrt{\frac{2r\Lambda}{3} (2\pi - r\theta) \sin \theta \frac{\left(\sin^2 \frac{\theta_0}{2} - \sin^2 \frac{\theta_q}{2} \right) \left(\sin^2 \frac{\theta_0}{2} - \sin^2 \frac{\theta}{2} \right)}{\sin^2 \frac{\theta}{2} - \sin^2 \frac{\theta_q}{2}}}. \quad (5.5)$$

where the upper (lower) sign corresponds to an expanding (contracting) universe. Integrating Eq. (5.5) numerically for the initial condition

$$\theta(0) = \theta_0, \quad (5.6)$$

we obtain numerical solutions for the dihedral angle. In Fig. 4 we give the plots of dihedral angles for the six types of regular 4-polytopes. They are monotone decreasing functions of time for $0 \leq t \leq \tau_{p,q,r}/2$ and approach θ_q as $t \rightarrow \tau_{p,q,r}/2$, where $\tau_{p,q,r}$ is defined by

$$\tau_{p,q,r} = 2 \int_{\theta_q}^{\theta_0} d\theta \frac{2\pi - r(\theta - \sin \theta)}{2 \sin \frac{\theta}{2} \csc \frac{\theta_0}{2}} \sqrt{\frac{3 \left(\sin^2 \frac{\theta}{2} - \sin^2 \frac{\theta_q}{2} \right)}{2r\Lambda (2\pi - r\theta) \left(\sin^2 \frac{\theta_0}{2} - \sin^2 \frac{\theta_q}{2} \right) \left(\sin^2 \frac{\theta_0}{2} - \sin^2 \frac{\theta}{2} \right) \sin \theta}}. \quad (5.7)$$

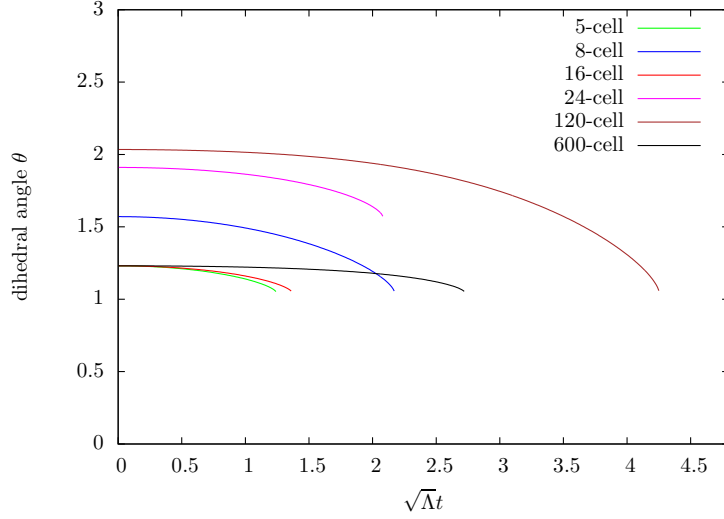


Figure 4: Plots of the dihedral angles of the regular 4-polytope models. Each plot ends at $t = \tau_{p,q,r}/2$.

As noted above, the edge length becomes the maximum value $l = l_{p,q,r}$ at $t = \tau_{p,q,r}/2$. After reaching $l_{p,q,r}$, one of the most reasonable and easiest way is that the edge length begins to decrease. The differential equation for the dihedral angle (5.5) changes its sign to positive at the terminal time $\tau_{p,q,r}/2$, then the universe begins to contract. It continues until the edge length reaches the initial minimum value $l = l_0$ at $t = \tau_{p,q,r}$. The universe begins to expand again, repeating expansion and contraction with a period $\tau_{p,q,r}$. On the condition (4.8), the velocity \dot{l} diverges at the time $\tau_{p,q,r}/2$. The edge length l varies in the range $l_0 \leq l \leq l_{p,q,r}$. Therefore there is no smooth continuation to the scale factor for $t \geq \tau_{p,q,r}/2$. If we employ another initial condition for the evolution equation, positions of spikes are shifted, but do not disappear. Thus the spikes surely come in the time evolution of the scale factor.

For comparison with the continuum theory, we introduce an analog of the scale factor $a(t)$. Here, we simply define the scale factor of the polytopal universe a_R as the radius of the circumsphere of the regular polytope

$$\begin{aligned}
 a_R(t) &= \frac{l(t)}{2} \sqrt{\frac{\sin^2 \frac{\pi}{q} - \cos^2 \frac{\pi}{r}}{\sin^2 \frac{\pi}{p} \sin^2 \frac{\pi}{r} - \cos^2 \frac{\pi}{q}}} \\
 &= \sqrt{\frac{3 \cot \frac{\theta}{2} (2\pi - r\theta) \left(\sin^2 \frac{\pi}{r} - \sin^2 \frac{\theta_q}{2} \right)}{r\Lambda \left(\sin^2 \frac{\theta_0}{2} - \sin^2 \frac{\theta_q}{2} \right) \left(\sin^2 \frac{\pi}{r} - \sin^2 \frac{\theta_0}{2} \right)}} \sin \frac{\theta_0}{2}. \tag{5.8}
 \end{aligned}$$

In Fig. 5 we give the plots of the scale factors of the regular 4-polytopal universes as functions of time. The broken curve corresponds to the continuum solution. One can see that the regular 4-polytopal solutions approximate the continuum solution for $\sqrt{\Lambda t} < 1$. In particular, the more vertices the polytope contains, the better approximation is achieved.

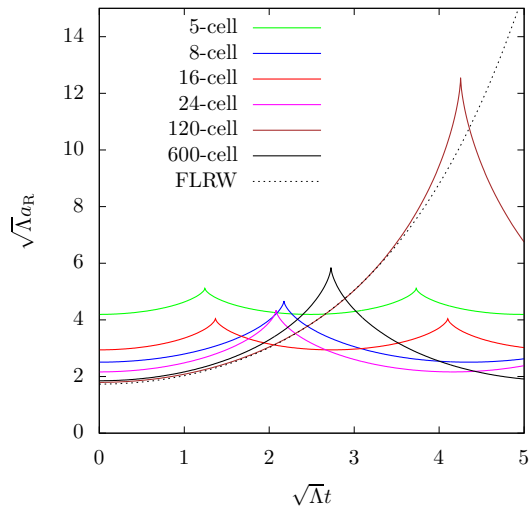


Figure 5: Plots of the scale factors of the regular 4-polytope models.

That the numerical solutions reproduce the behavior of the continuum solution well for $\sqrt{\Lambda}t < 1$ can be understood by noting the fact that the scale factor (5.8) approximately satisfies the Friedmann equations (2.3) when both $\sqrt{\Lambda}l$ and \dot{l} are small. In fact, the Hamiltonian constraint (4.9) and the evolution equation (4.10) can be approximated as

$$\frac{\Lambda}{3}l^2 - \dot{l}^2 = \frac{\Lambda}{3}l_0^2, \quad \ddot{l} = \frac{\Lambda}{3}l. \quad (5.9)$$

The deviations from the continuum solution, however, get large with time. In particular the polytopal universes repeat expansion and contraction. This is a unique characteristic of the polytope models. It cannot be seen in the FLRW universe or polyhedral universes.

6 Noninteger Schläfli symbol and pseudo-regular 4-polytopal universes

In the previous section, we investigated the behaviors of the regular 4-polytopal universes. We have shown that the universes repeat expansion and contraction periodically. This property cannot be seen in an FLRW universe of the continuum general relativity. In the rest of this paper we are concerned with the issue of whether the model recovers the FLRW universe in the continuum limit, or not. A straightforward way to implement the continuum limit is to introduce an extension of the geodesic domes we have considered for polyhedron models [11].

To better approximate a sphere beyond regular polyhedra we considered geodesic domes in Ref. [11]. We now extend them to 4-polytopes. To define a four-dimensional geodesic

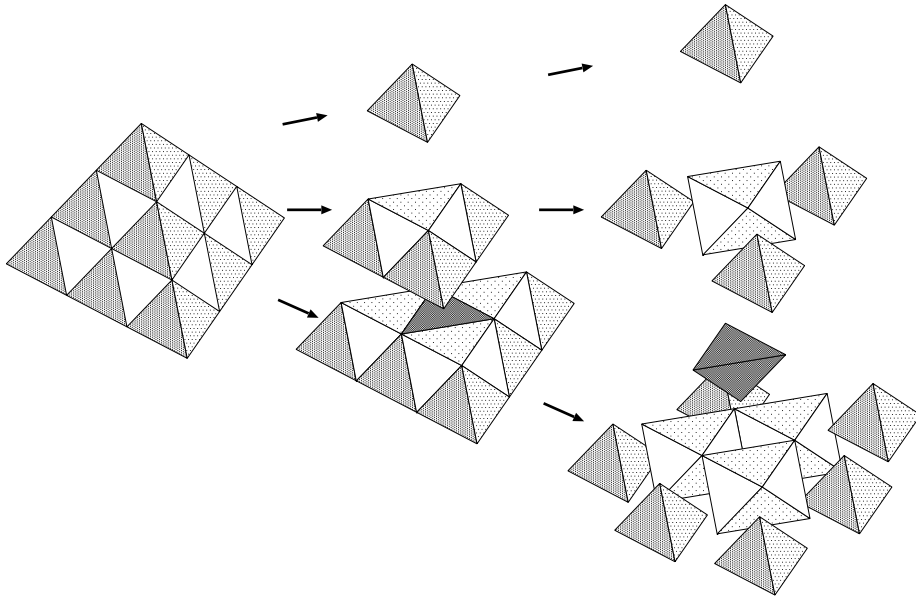


Figure 6: Subdivision of a regular tetrahedron in the case of $\nu = 3$.

dome, geodesic 4-dome in brief, we divide each cell of a regular polytope into smaller polyhedra. By projecting the vertices of the subdivided cells on to the circumsphere of the original regular polytope we can define a geodesic 4-dome, a polytope having the points projected on to the circumsphere as the vertices. The method of subdivision is rather arbitrary and depends on the regular polyhedron to be subdivided. In Ref. [7], Brewin proposed a subdivision of a tetrahedron into tetrahedra that are not regular. Here we require that the subdivision of a regular polyhedron should yield regular polyhedra of equal edge length. In fact, a cube can be subdivided into ν^3 smaller cubes of edge of a one- ν th edge length, where ν is a positive integer called “frequency”. Similarly, a regular tetrahedron and octahedron can be subdivided into smaller regular tetrahedra and octahedra as illustrated in Fig. 6 for a regular tetrahedron. We can then construct geodesic 4-domes by applying these subdivisions to regular polytopes except for 120-cell. Since a dodecahedron has no subdivision into smaller regular polyhedra, we will not consider geodesic 4-domes for 120-cell.

Regge calculus for the geodesic 4-domes becomes cumbersome as the frequency ν increases as we have shown in Ref. [11] in three dimensions. We can avoid this by regarding the geodesic 4-domes as pseudo-regular 4-polytopes described by a non-integer Schläfli symbol. In what follows we consider as the polytopal universe pseudo-regular 4-polytopes corresponding to 600-cell-based geodesic 4-domes. We first define the Schläfli symbol characterizing pseudo-regular 4-polytopes.

For our purpose we summarize the numbers of cells, faces, edges, and vertices of the geodesic 4-dome in Table 3. At a frequency ν each cell of a 600-cell can be subdivided into $\nu(\nu^2 + 2)/3$ tetrahedra and $\nu(\nu^2 - 1)/6$ octahedra as depicted in Fig. 6. The geodesic 4-dome is then obtained by projecting the 600-cell tessellated by the $300(\nu^2 + 1)$ tiles on

Frequency		ν
N_3	Tetrahedra	$200\nu(\nu^2 + 2)$
	Octahedra	$100\nu(\nu^2 - 1)$
	Total	$300\nu(\nu^2 + 1)$
N_2	Tetra-Tetra connectors	$600\nu(\nu + 1)$
	Octa-Octa connectors	$600\nu(\nu - 1)$
	Tetra-Octa connectors	$400\nu(2\nu^2 - 3\nu + 1)$
	Total	$400\nu(2\nu^2 + 1)$
N_1	Five-way connectors	720ν
	Four-way connectors	$600\nu(\nu^2 - 1)$
	Total	$120\nu(5\nu^2 + 1)$
N_0		$20\nu(5\nu^2 + 1)$

Table 3: Numbers of cells, faces, edges, and vertices of a four-dimensional geodesic dome.

to the circumsphere. It has three types of triangular faces: one is a common face of two tetrahedra, another shared by two octahedra, and the other connecting a tetrahedron with an octahedron. Let us call them ‘‘Tetra-Tetra connectors’’, ‘‘Octa-Octa connectors’’, and ‘‘Tetra-Octa connectors’’, respectively. Furthermore, there are two types of edges. One is shared by five cells. They are coming from the edges of the original regular 600-cell. The other type of edges is shared by four cells. They correspond to newly generated edges by subdividing tetrahedral cells. Let us call the former type of edges ‘‘five-way connectors’’ and the latter ‘‘four-way connectors’’, respectively.

A naive way to define the Schläfli symbol $\{p, q, r\}$ for the pseudo-regular polytope is taking the average number of edges of a face as p , of faces around a vertex in a cell as q , and of cells around an edge as r . This leads to

$$\{p, q, r\} = \left\{ 3, \frac{12(2\nu^2 + 1)}{7\nu^2 + 5}, \frac{10(2\nu^2 + 1)}{5\nu^2 + 1} \right\}. \quad (6.1)$$

Pseudo-regular polytopes corresponding to the fractional Schläfli symbol (6.1), however, do not approach the three-dimensional sphere S^3 in the infinite frequency limit. This can be seen by noting the fact that a deficit angle ε around an edge of a regular polytope is given by $\varepsilon = 2\pi - 2r \arcsin[\cos(\pi/q) / \sin(\pi/p)]$. When applied to the pseudo-regular polytope, the deficit angle should satisfy $\varepsilon \rightarrow 0$ for $\nu \rightarrow \infty$ or $\{p, q, r\} \rightarrow \{3, 24/7, 4\}$. It is obvious that this is not the case. Such a discrepancy happens since the subdivision of a cell involves two types of polyhedra: tetrahedra and octahedra. If we considered an 8-cell-based geodesic

4-dome, we could obtain a pseudo-regular polytope characterized by a fractional Schläfli symbol having a limit $\{p, q, r\} \rightarrow \{4, 3, 4\}$.

What we have shown is that the idea of averaging the Schläfli symbols does not work except for an 8-cell-based geodesic 4-dome. We must employ another method of averaging to define Schläfli symbols that not only have a smooth continuum limit but also preserve the geometrical characteristics of polytopes.

To achieve this goal we introduce a set of angles ϑ_2 , ϑ_3 , and ϑ_4 , where ϑ_2 is an interior angle of a face of a regular polytope $\{p, q, r\}$, ϑ_3 a dihedral angle of two adjacent faces, and ϑ_4 a hyperdihedral angle between two neighboring cells. They can be written in terms of p , q , and r as

$$\vartheta_2 = \frac{p-2}{p}\pi = 2 \arcsin \left(\cos \frac{\pi}{p} \right), \quad (6.2)$$

$$\vartheta_3 = 2 \arcsin \left(\frac{\cos \frac{\pi}{q}}{\sin \frac{\pi}{p}} \right), \quad (6.3)$$

$$\vartheta_4 = 2 \arcsin \left(\frac{\sin \frac{\pi}{p} \cos \frac{\pi}{r}}{\sqrt{\sin^2 \frac{\pi}{p} - \cos^2 \frac{\pi}{q}}} \right). \quad (6.4)$$

These can be solved with respect to the Schläfli symbol as

$$p(\vartheta_2) = \frac{\pi}{\arccos \left(\sin \frac{\vartheta_2}{2} \right)}, \quad (6.5)$$

$$q(\vartheta_2, \vartheta_3) = \frac{\pi}{\arccos \left(\cos \frac{\vartheta_2}{2} \sin \frac{\vartheta_3}{2} \right)}, \quad (6.6)$$

$$r(\vartheta_3, \vartheta_4) = \frac{\pi}{\arccos \left(\cos \frac{\vartheta_3}{2} \sin \frac{\vartheta_4}{2} \right)}. \quad (6.7)$$

We are now able to extend the Schläfli symbol to an arbitrary pseudo-regular polytope by substituting in Eqs. (6.5)–(6.7) the angles $\vartheta_{2,3,4}$ with averaged ones of tessellated parent regular polytopes. With the help of Table 3, it is straightforward to obtain the averaged angles of tessellated 600-cell as

$$\vartheta_2 = \frac{\pi}{3}, \quad (6.8)$$

$$\vartheta_3 = \frac{(\nu^2 - 1)\pi + 3 \arccos \frac{1}{3}}{2\nu^2 + 1}, \quad (6.9)$$

$$\vartheta_4 = \frac{(2\nu^2 - 3\nu + 1)\pi + 3\nu \arccos \left(-\frac{3\sqrt{5}+1}{8} \right)}{2\nu^2 + 1}. \quad (6.10)$$

The pseudo-regular 4-polytope with the Schläfli symbol (Eqs. 6.5–6.10) has a smooth S^3 limit for $\nu \rightarrow \infty$ since $\{p, q, r\} \rightarrow \{3, \pi / \arccos(\sqrt{6}/4), 4\}$ and, hence, the deficit angle around an edge of a pseudo-regular 4-polytope satisfies $\varepsilon = 2\pi - 2r \arcsin [\cos(\pi/q) / \sin(\pi/p)] \rightarrow 0$.

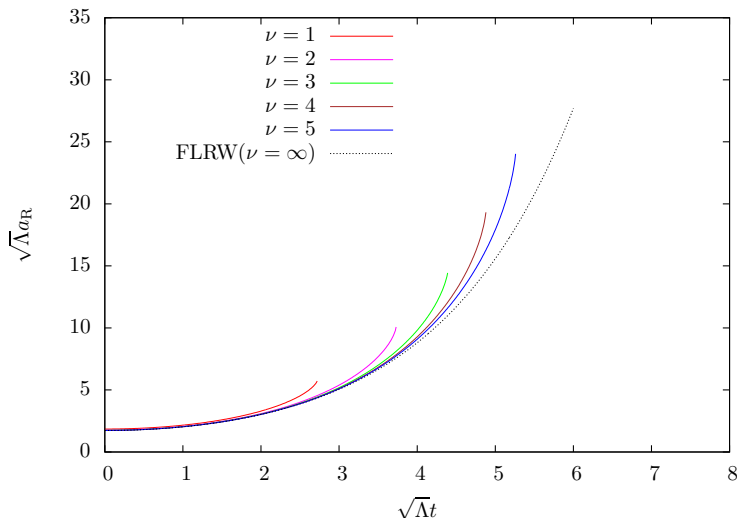


Figure 7: Plots of the scale factors of the pseudo-regular 4-polytope models for $\nu \leq 5$.

Assuming that the expression for the scale factor (5.8) can be applied to the pseudo-regular 4-polytopal universe with the non-integer Schläfli symbol defined by Eqs. (6.5)–(6.10), we can immediately obtain numerical solutions for an arbitrary frequency ν . In Fig. 7 we give plots of the scale factors for $\nu \leq 5$ and $0 \leq t \leq \tau_{p,q,r}/2$. It can easily be seen that the pseudo-regular 4-polytope model approaches the FLRW universe as the frequency increases. The universe oscillates periodically for finite frequencies but the maximum scale factor and the period of oscillation grow with ν . The scale factor for $\nu = 100$ is shown in Fig. 8. That the Regge equations for the pseudo-regular 4-polytope reproduce the Friedmann equations (2.3) in the infinite frequency limit can be directly seen by substituting the scale factor (5.8) for the Hamiltonian constraint (4.9) and the evolution equation (4.10), and then taking the limit $\{p, q, r\} \rightarrow \{3, \pi/\arccos(\sqrt{6}/4), 6\}$.

7 Summary and discussions

We have investigated a four-dimensional closed FLRW universe with a positive cosmological constant using the CW formalism in Regge calculus. The main objective of this work is to extend the approach developed in Ref. [11] for three-dimensional models to four dimensions. In particular, generalization of the method of pseudo-regular polyhedra and fractional Schläfli symbol is our prime concern.

The three-dimensional hyperspherical Cauchy surfaces of the continuum FLRW universe are replaced with regular 4-polytopes instead of regular polyhedra in three-dimensional models. In four dimensions, the curvature reveals itself as deficit angles around hinges of two-dimensional faces. This makes the task in carrying out Regge calculus a bit cumbersome.

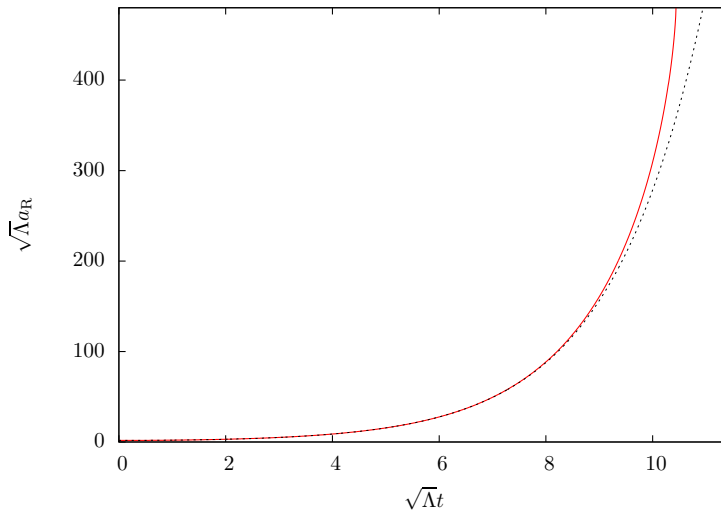


Figure 8: Plot of the scale factor of the pseudo-regular 4-polytope model for $\nu = 100$. The broken curve is corresponding to the continuum FLRW universe.

We can handle the matter for all six types of regular 4-polytopes in a unified way in terms of the Schläfli symbol. We have seen that discretized universe changes the behavior according to the space-time dimensions. In the case of polyhedral universe the scale factor becomes infinite in a finite time. This is because the dihedral angle corresponding to Eq. (5.1) approaches zero in a finite time as the universe expands to infinity. In four dimensions the polytopal universe stops expanding with a finite edge length in a finite time and then begins to contract to the scale where the universe starts expansion again. We thus arrive at a picture of an oscillating universe.

To go beyond the regular polytopes we have introduced pseudo-regular polytopes and a non-integer Schläfli symbol as a substitute of geodesic 4-domes. The fractional Schläfli symbol introduced in Ref. [11] for the pseudo-regular polyhedra is defined by averaging the data such as the number of faces that have a vertex in common. When applied to pseudo-regular polytopes, the fractional Schläfli symbol does not recover a smooth three-dimensional sphere in the infinite frequency limit. To get rid of this difficulty we have employed averaged dihedral angles to define the Schläfli symbol by using Eqs. (6.5)–(6.7). It is neither integral nor fractional. We have shown that the continuum FLRW universe can be reproduced in the infinite frequency limit of the oscillating polytopal universe.

Our concern in this work is restricted to the vacuum solution of Einstein gravity with a positive cosmological constant. Furthermore, we have assumed compact hyperspherical Cauchy surfaces corresponding to positive curvature parameter. Inclusion of non-hyperspherical Cauchy surfaces as well as gravitating matter would certainly be interesting. We can also apply the approach of pseudo-regular polytopes to a higher-dimensional FLRW universe. In $D(> 4)$ dimensions there are only three types of regular polytopes: D -simplex,

D -cube, and D -orthoplex, as mentioned in Appendix A. We expect that this makes the Regge calculus of polytopal universes in five or more dimensions easier.

Acknowledgments

The authors would like to thank Y. Hyakutake, N. Motoyui, M. Sakaguchi, and S. Tomizawa for useful discussions.

A Circumradius of a regular D -polytope

For a regular 4-polytope $\{p, q, r\}$, the Schläfli symbol can be written in terms of dihedral angles as Eqs. (6.5)–(6.7). For a regular D -polytope $\{p_2, \dots, p_D\}$, if we introduce $\vartheta_0 = \vartheta_1 = 0$ and denote by ϑ_i a dihedral angle of an i -dimensional face for $i \geq 2$, we can express the relation between Schläfli symbol and dihedral angles generally, as

$$p_i = \frac{\pi}{\arccos\left(\cos\frac{\vartheta_{i-1}}{2} \sin\frac{\vartheta_i}{2}\right)}. \quad (\text{A.1})$$

As can be seen from Eq. (A.1), the Schläfli symbol can be extended for $i = 0, 1$ as $p_0 = p_1 = 2$. Then, a regular D -polytope can be associated with a set of $D+1$ parameters $\{p_0, p_1, \dots, p_D\}$.

Let us denote half the length of a line segment by R_1 , and the radius of the circumsphere of a D -polytope by R_D . Using an extended Schläfli symbol $\{p_0, p_1, \dots, p_D\}$, we can write the first four of the circumradii as

$$R_1 = \frac{l}{2} \sqrt{\frac{\sin^2 \frac{\pi}{p_1}}{\sin^2 \frac{\pi}{p_0}}}, \quad (\text{A.2})$$

$$R_2 = \frac{l}{2} \sqrt{\frac{\sin^2 \frac{\pi}{p_1}}{\sin^2 \frac{\pi}{p_0} \sin^2 \frac{\pi}{p_2}}}, \quad (\text{A.3})$$

$$R_3 = \frac{l}{2} \sqrt{\frac{\sin^2 \frac{\pi}{p_1} \sin^2 \frac{\pi}{p_3}}{\sin^2 \frac{\pi}{p_0} \left(\sin^2 \frac{\pi}{p_2} - \cos^2 \frac{\pi}{p_3}\right)}}, \quad (\text{A.4})$$

$$R_4 = \frac{l}{2} \sqrt{\frac{\sin^2 \frac{\pi}{p_1} \left(\sin^2 \frac{\pi}{p_3} - \cos^2 \frac{\pi}{p_4}\right)}{\sin^2 \frac{\pi}{p_0} \left(\sin^2 \frac{\pi}{p_2} \sin^2 \frac{\pi}{p_4} - \cos^2 \frac{\pi}{p_3}\right)}}, \quad (\text{A.5})$$

where l is the edge length of the regular polytopes.

From Eqs. (A.2)–(A.5), the recurrence relations for the circumradii can be guessed. In

	Regular simplex	Hypercube	Orthoplex
$\{p_2\}$	$\{3\}$	$\{4\}$	$\{4\}$
$\{p_2, p_3\}$	$\{3, 3\}$	$\{4, 3\}$	$\{3, 4\}$
$\{p_2, p_3, p_4\}$	$\{3, 3, 3\}$	$\{4, 3, 3\}$	$\{3, 3, 4\}$
$\{p_2, p_3, \dots, p_{D-1}, p_D\}$	$\{3, 3, \dots, 3, 3\}$	$\{4, 3, \dots, 3, 3\}$	$\{3, 3, \dots, 3, 4\}$
R_D	$\sqrt{\frac{D}{2(D+1)}}l$	$\frac{\sqrt{D}}{2}l$	$\frac{\sqrt{2}}{2}l$

Table 4: The Schläfli symbols and the circumradii of regular simplices, hypercubes, and orthoplices. l is an edge length of the polytopes.

the expression of R_i , letting

$$\begin{cases} \sin^2 \frac{\pi}{p_{i-1}} & \rightarrow \sin^2 \frac{\pi}{p_{i-1}} \sin^2 \frac{\pi}{p_{i+1}} \\ \cos^2 \frac{\pi}{p_{i-1}} & \rightarrow \cos^2 \frac{\pi}{p_{i-1}} \sin^2 \frac{\pi}{p_{i+1}} \\ \sin^2 \frac{\pi}{p_{i-2}} & \rightarrow \sin^2 \frac{\pi}{p_{i-2}} \left(1 - \csc^2 \frac{\pi}{p_i} \cos^2 \frac{\pi}{p_{i+1}}\right) \\ \cos^2 \frac{\pi}{p_{i-2}} & \rightarrow \cos^2 \frac{\pi}{p_{i-2}} \left(1 - \csc^2 \frac{\pi}{p_i} \cos^2 \frac{\pi}{p_{i+1}}\right) \end{cases}, \quad (\text{A.6})$$

then we obtain the expression of R_{i+1} . For the reader's reference we give the next three circumradii:

$$R_5 = \frac{l}{2} \sqrt{\frac{\sin^2 \frac{\pi}{p_1} \left(\sin^2 \frac{\pi}{p_3} \sin^2 \frac{\pi}{p_5} - \cos^2 \frac{\pi}{p_4} \right)}{\sin^2 \frac{\pi}{p_0} \left(\sin^2 \frac{\pi}{p_2} \left(\sin^2 \frac{\pi}{p_4} - \cos^2 \frac{\pi}{p_5} \right) - \cos^2 \frac{\pi}{p_3} \sin^2 \frac{\pi}{p_5} \right)}}, \quad (\text{A.7})$$

$$R_6 = \frac{l}{2} \sqrt{\frac{\sin^2 \frac{\pi}{p_1} \left(\sin^2 \frac{\pi}{p_3} \left(\sin^2 \frac{\pi}{p_5} - \cos^2 \frac{\pi}{p_6} \right) - \cos^2 \frac{\pi}{p_4} \sin^2 \frac{\pi}{p_6} \right)}{\sin^2 \frac{\pi}{p_0} \left(\sin^2 \frac{\pi}{p_2} \left(\sin^2 \frac{\pi}{p_4} \sin^2 \frac{\pi}{p_6} - \cos^2 \frac{\pi}{p_5} \right) - \cos^2 \frac{\pi}{p_3} \left(\sin^2 \frac{\pi}{p_5} - \cos^2 \frac{\pi}{p_6} \right) \right)}}, \quad (\text{A.8})$$

$$R_7 = \frac{l}{2} \sqrt{\frac{\sin^2 \frac{\pi}{p_1} \left(\sin^2 \frac{\pi}{p_3} \left(\sin^2 \frac{\pi}{p_5} \sin^2 \frac{\pi}{p_7} - \cos^2 \frac{\pi}{p_6} \right) - \cos^2 \frac{\pi}{p_4} \left(\sin^2 \frac{\pi}{p_6} - \cos^2 \frac{\pi}{p_7} \right) \right)}{\sin^2 \frac{\pi}{p_0} \left(\sin^2 \frac{\pi}{p_2} \left(\sin^2 \frac{\pi}{p_4} \left(\sin^2 \frac{\pi}{p_6} - \cos^2 \frac{\pi}{p_7} \right) - \cos^2 \frac{\pi}{p_5} \sin^2 \frac{\pi}{p_7} \right) - \cos^2 \frac{\pi}{p_3} \left(\sin^2 \frac{\pi}{p_5} \sin^2 \frac{\pi}{p_7} - \cos^2 \frac{\pi}{p_6} \right) \right)}}, \quad (\text{A.9})$$

It is well known that in five or higher dimensions there are only three types of regular polytopes: regular simplex, hypercube, and orthoplex. Hereafter we restrict our investigation to these regular polytopes. We summarize the Schläfli symbols and circumradii of the polytopes in Table 4. As can be seen from this table, the circumradii are written as simple functions in terms of dimension D . Therefore the recurrence relations (A.6) can easily be inspected numerically. In fact, we have put it into practice and confirmed the correctness for $D \leq 50$.

As can also be seen from Table 4, D -simplex, D -cube, and D -orthoplex have the Schläfli symbol $p_3 = \dots = p_{D-1} = 3$ in common. Thus in five or higher dimensions a general form of the circumradii of the D -polytopes might be given as a function of a set of three parameters $\{D, p_2, p_D\}$. Substituting $p_0 = p_1 = 2$ and $p_3 = \dots = p_{D-1} = 3$ into the functions generated by the recurrence relations (A.6) and the initial condition (A.2), and comparing

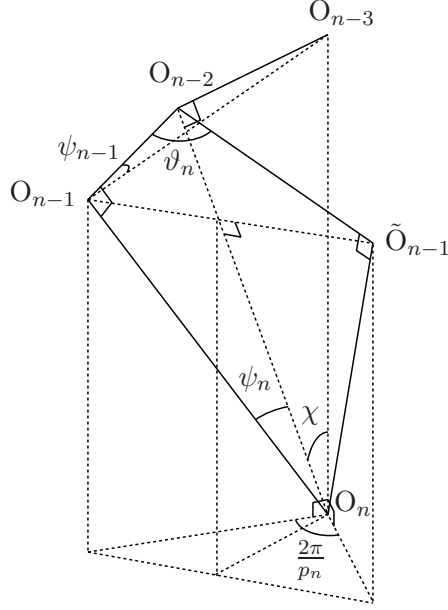


Figure 9: O_n is the circumcenter of Π_n . O_{n-1} and \tilde{O}_{n-1} are the centers of two $(n-1)$ -dimensional faces sharing Π_{n-2} centered at O_{n-2} , and O_{n-3} is located at the center of Π_{n-3} .

the expressions, we can guess the general form of the circumradius of a regular D -polytope;

$$R_D = \frac{l}{2} \sqrt{\frac{(D-2) \cos \frac{2\pi}{p_D} - 1}{\cos \frac{2\pi}{p_2} - \frac{D-3}{2} \cos \left(\frac{2\pi}{p_2} - \frac{2\pi}{p_D} \right) - \frac{D-3}{2} \cos \left(\frac{2\pi}{p_2} + \frac{2\pi}{p_D} \right) + \cos \frac{2\pi}{p_D}} \quad (D = 5, 6, 7, \dots). \quad (\text{A.10})$$

Assigning $\{p_2, p_D\} = \{3, 3\}, \{4, 3\}, \{3, 4\}$ to Eq. (A.10), the circumradii of D -simplex, D -cube, and D -orthoplex are reproduced, respectively.

Note added in proof

At the end of this paper, we give a short account of the relation between Schläfli symbol and dihedral angles (A.1). We consider an arbitrary regular n -polytope $\{p_0, p_1, p_2, \dots, p_n\}$ and denote it by Π_n , where p_0 and p_1 are introduced in Appendix A. Π_n has regular $(n-1)$ -polytopes $\{p_0, p_1, \dots, p_{n-1}\}$ as $(n-1)$ -dimensional faces. Similarly each k -dimensional face Π_k has regular polytopes Π_{k-1} for $n \geq k \geq 1$.

Let us choose a set of faces $\Pi_0, \Pi_1, \dots, \Pi_n$ satisfying $\Pi_0 \subset \Pi_1 \subset \dots \subset \Pi_n$ and denote by O_k the center of circumsphere of the Π_k ($n \geq k \geq 0$). Furthermore we define the angles

$$\psi_n = \angle O_{n-2} O_n O_{n-1}, \quad \psi_{n-1} = \angle O_{n-3} O_{n-1} O_{n-2}, \quad \chi = \angle O_{n-3} O_n O_{n-2}. \quad (\text{A.11})$$

As can be seen from Fig. 9, these satisfy

$$\tan \chi = \sin \psi_n \tan \psi_{n-1}, \quad \tan \psi_n = \sin \chi \tan \frac{\pi}{p_n}, \quad \vartheta_n = \pi - 2\psi_n, \quad (\text{A.12})$$

and from which we obtain Eq. (A.1).

References

- [1] T. Regge, *Il Nuovo Cim.* **19**, 558 (1961).
- [2] C. W. Misner, K. S. Thorne, and J. A. Wheeler, in *Gravitation* (Freeman, New York, 1973), Chap. 42.
- [3] J. W. Barrett, D. Oriti, and R. M. Williams, [arXiv:1812.06193 [gr-qc]].
- [4] P. A. Collins and R. M. Williams, *Phys. Rev.* **D 7**, 965 (1973).
- [5] R. Arnowitt and S. Deser, *Phys. Rev.* **113**, 745 (1959).
- [6] R. Arnowitt, S. Deser, and C. W. Misner, *Phys. Rev.* **116**, 1322 (1959).
- [7] L. Brewin, *Class. Quant. Grav.* **4**, 899 (1987).
- [8] R. G. Liu and R. M. Williams, *Phys. Rev.* **D 93**, 024032 (2016) [arXiv:1501.07614[gr-qc]].
- [9] R. G. Liu and R. M. Williams, *Phys. Rev.* **D 93**, 023502 (2016) [arXiv:1502.03000[gr-qc]].
- [10] R. G. Liu and R. M. Williams, [arXiv:1510.05771[gr-qc]].
- [11] R. Tsuda and T. Fujiwara, *Prog. Theor. Exp. Phys.* **2017**, 073E01 (2017) [arXiv:1612.06536[gr-qc]].
- [12] H. S. M. Coxeter, *Regular Polytopes* (Dover Publications, Inc., New York, 1973).
- [13] W. A. Miller, *Class. Quant. Grav.* **14**, 199 (1997) [arXiv:gr-qc/9708011].
- [14] L. Schläfli, *Quart. J. Pure Appl. Math.* **2**, 269 (1858).
- [15] H. M. Haggard, A. Hedeman, E. Kur, and R. G. Littlejohn, *J. Phys. A: Math. Theor.* **48**, 105203 (2015) [arXiv:1409.7117 [math-ph]].
- [16] S. Hitotsumatsu, in *Kōjigen No Seitamentai (Regular polyhedra in higher dimensions)* (Nippon Hyoron Sha Co., Ltd, 1983), Chap. 5.